Title: ***Combinatorial polymeric conjugated micelles with dual cytotoxic and antiangiogenic effects for the treatment of ovarian cancer***

Authors: Deepa A. Rao[1], Gyan Mishra[2], Bhuvana Shyam Doddapaneni[2], Sergiy Kyryachenko[2], Igor H. Wierzbicki[2], Duc X Ngyuen[2], Vidhi Shah[2], Adel M. Al Fatease[2], Raid G Alany[3], Adam WG Alani[2,*]

[1]School of Pharmacy, Pacific University, Hillsboro OR, USA

[2]Department of Pharmaceutical Sciences, College of Pharmacy, Oregon State University, Portland OR, USA

[3]School of Pharmacy and Chemistry, Drug Discovery, Delivery and Patient Care (DDDPC) Theme, Kingston University, London, UK

[*]Corresponding author: 2730 SW Moody Ave, Portland, OR 97201; Tel: (503) 346-4702, Email: adam.alani@oregonstate.edu

Abstract

Emerging treatment paradigms like targeting the tumor microenvironment and/or dosing as part of a metronomic regimen are anticipated to produce better outcomes in ovarian cancer but current drug delivery systems are lacking. We have designed and evaluated paclitaxel (PTX) and rapamycin (RAP) micellar systems that can be tailored for various dosing regimens and target tumor microenvironment. Individual and mixed PTX:RAP (MIX-M) micelles are prepared by conjugating drugs to a poly(ethylene glycol)-block-poly(β-benzyl L-aspartate) using a pH-sensitive linker. The micelles release the drug(s) at pH 5.5 indicating preferential release in the acidic endosomal/lysosomal environment. Micelles exhibit anti-proliferative effects in ovarian cell cancer lines (SKOV-3 and ES2) and an endothelial cell line (HUVEC) with the MIX-M being synergistic. The micelles also inhibited endothelial migration and tube formation. In healthy mice, micelles at 60 mg/kg/drug demonstrated no acute toxicity over 21 days. ES2 xenograft model efficacy studies at 20 mg/kg/drug dosed every 4 days and evaluated at 21 days indicate that the individual micelles exhibit anti-angiogenic effects, while the MIX-M exhibited both anti-angiogenic and apoptotic induction that results in significant tumor volume reduction. Based on our results, MIX-M micelles can be utilized to achieve synergistic apoptotic and anti-angiogenic effects when treated at frequent low doses.

1. Introduction

Epithelial ovarian cancer is the most lethal gynecologic malignancy in the United States[1] due to the complexity of the disease which results in a high rate of recurrence and the development of chemo-resistant disease. The response rate for recurrent ovarian cancer is 30% for most patients and the rate is even lower in those women who become refractory to platinum compounds[2]. Current chemotherapeutic strategies for treatment rely on maximum tolerated doses (MTD) of taxanes and platinums administered every 3 weeks[3, 4]. This allows for an extended drug-free period for the patient to recover from chemotherapy-induced adverse effects. However, this drug-free interval can also result in tumor reinitiating growth[5] through the mobilization of circulating endothelial progenitor cells and results in tumor neovascularization and lower longer term prognosis[3]. MTD treatment in advanced ovarian cancer (stages III and IV) also results in frequent discontinuation of therapy because of toxicity and/or development of resistance[6, 7].

New advances in tumor biology suggest targeting the tumor microenvironment and not just the cancer cells[8, 9]. This is backed by emerging clinical data that indicates that antiangiogenic agents can induce ovarian tumor regression; however, resistance and toxicity develop quickly[10-14]. Newer, therapeutic paradigms like metronomic therapy has been developed to target tumor cells and microenvironment. Metronomic therapy as defined by the administration of chemotherapeutic agents at doses significantly below the MTD, given at regular, more frequent time intervals with no prolonged drug-free breaks[15-17]. The basis of the metronomic dosing regimen (MR) lies in shifting cancer treatment from an acute response (MTD treatment) to management as a chronic condition. The second goal of MR is to target not only the cancer cells directly but also the surrounding new vasculature that emerges through angiogenesis[3, 16, 18, 19]. In addition, new studies have shown that MR induces other mechanisms of action including antitumor immune responses and direct anticancer effects. Therefore, MR is now considered to be a form of multiple-targeted chemotherapy that has a profound effect on the tumor microenvironment[20]. Many studies have demonstrated that patients with advanced cancer who developed resistance to MTD chemotherapy could still benefit from iterative dosing of distinct cytotoxic drugs utilizing MR, at a tenth to a third of the MTD[21].

Currently no drug delivery systems exist for the treatment of ovarian cancer that can be adapted for conventional and emerging treatment paradigms without developing resistance and/or inducing toxicity. Agents commonly used in treating ovarian cancer include platinums and taxanes, while platinums have shown efficacy at MTD currently no data exists indicating platinums have any effect in inhibiting angiogenesis and affecting tumor microenvironment. Taxanes like paclitaxel (PTX) and other cancer cytotoxic agents like mammalian target of rapamycin (mTOR) inhibitors, have demonstrated both cytotoxic and secondary antiangiogenic effects in tumor tissues[22, 23]. However, these dual capacities are not fully manifested, due to limitations in dosing regimens and available drug formulations[18, 22, 24, 25]. PTX, a taxane, is a cytotoxic agent that causes stabilization of microtubule dynamics leading to cancer cell death[26], and can also inhibit endothelial cell proliferation, tube formation and migration[27, 28], thereby inhibiting the angiogenic process [29]. Rapamycin (RAP), an mTOR inhibitor, is another cytotoxic agent that can inhibit cancer cell proliferation and angiogenesis. RAP exerts its effect by acting

directly on mTOR, a key kinase acting downstream of the activation of PI3K[30], leading to the inhibition of VEGF expression and blocking the endothelial to mesenchymal transition. Evidence also links the inhibition of mTOR to the suppression of proangiogenic factors through down regulation of hypoxia mediated pathways[22, 31, 32].

Conventional dosing regimens of PTX and RAP are unable to sustain cytotoxic and antiangiogenic effects during required recovery periods. While MR with a single agent has sustained antiangiogenic effects due to continual treatment, cytotoxic effects are not seen. Taxol®, PTX's commercial formulation, cannot be used as an antiangiogenic agent because the drug is entrapped in the formulation leading to the reduction in PTX antiangiogenic activity. RAP is currently available as an oral drug product, for immune suppression in transplant patients, and is being investigated in several clinical trials as a chemotherapeutic agent [20] yet, no i.v. formulations of RAP currently exist. Several recent publications, ours and others, have demonstrated that that PTX and RAP when dosed together have strong synergistic effects *in vitro* and *in vivo*[33]. Inhibition of mTOR using RAP has also been shown to increase and prolong sensitivity of various cancer cells to PTX[34-36]. A drug delivery system capable of achieving the required cytotoxic and antiangiogenic effects through synergistic combinations of PTX and RAP may provide the necessary versatility needed to adapt to existing and emerging treatment paradigms without the current drawbacks of toxicity and resistance.

Polymeric micelles have the capacity to deliver multiple agents simultaneously and release of these molecules can be tailored through physical entrapment of chemical conjugation[37, 38]. Amphiphilic block copolymers (ABCs) spontaneously assemble into polymeric micelles that are nanoscopic with a core/shell architecture[37, 38]. Poly(ethylene glycol)-*block*-poly(β-benzyl L-aspartate) (PEG-PBLA) is an ABC that has been used as a starting point for polymeric micelles to deliver various chemotherapeutics[39, 40]. We have developed new pH-sensitive conjugated polymeric micellar nanocarriers that can be adapted for the delivery of chemotherapeutic agents[41, 42]. The rate of drug release can be tuned, using different linkers, and allows the formation of mixed micelles containing multiple drugs in the core for simultaneously delivery within the targeted cell to achieve additive/synergistic effects (Fig. 1)[42-45]. Therefore, we hypothesize that a polymeric micellar system that can simultaneously deliver PTX and RAP to provide both synergistic cytotoxic and antiangiogenic effects in an ovarian cancer mouse model can be adapted for conventional or emerging therapeutic strategies.

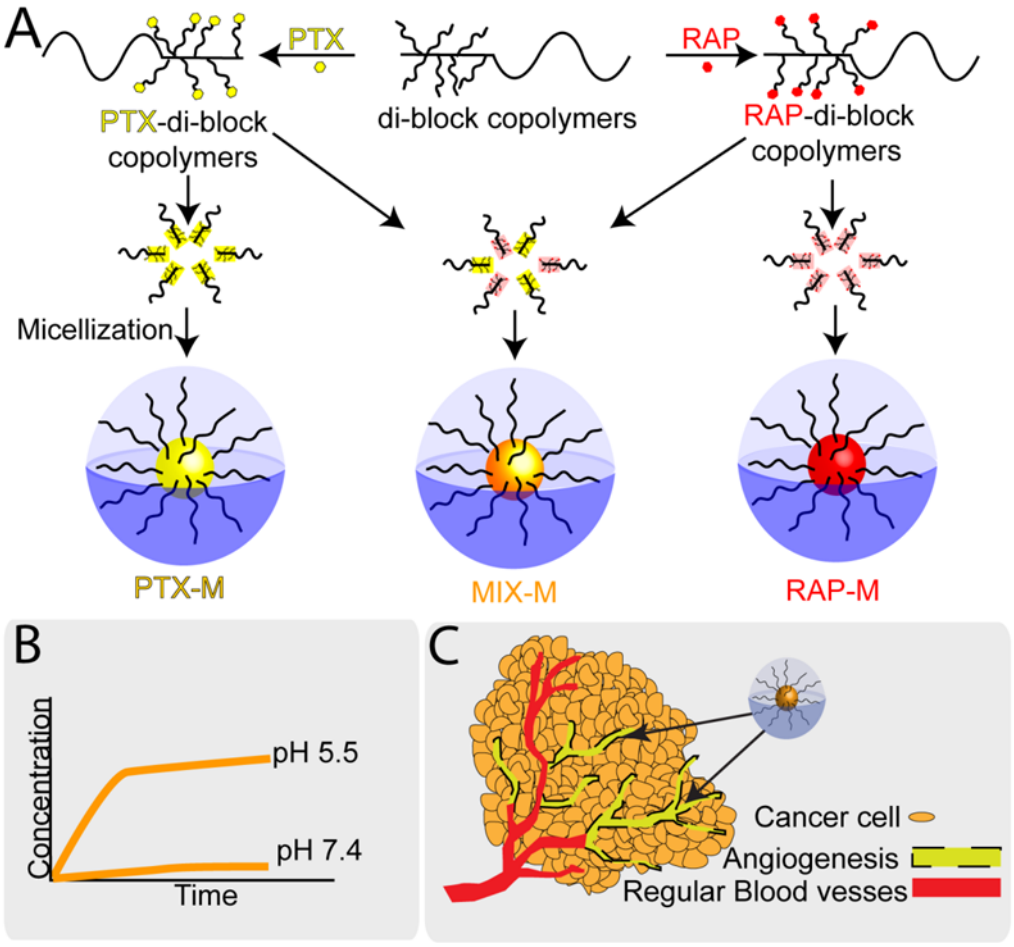

Fig. 1. Formation of PTX & RAP individual and mixed micelles (A). Theoretical pH-dependent drug release from micelles (B). Micelle accumulation in ovarian cancer cells and angiogenic vessels (C)

2. Materials & Methods

2.1. Materials

α-aminopropyl-ω-methoxy-poly(ethylene glycol) (PEG-NH_2) (Mn 12,000 g/mol, PDI = 1.03) was purchased from NOF America Corporation (White Plains, NY). PTX and RAP were obtained from LC laboratories Inc (Woburn, MA). Slide-A-Lyzer® dialysis cassettes (with a MWCO of 20,000 Da) were obtained from Thermo Scientific Inc. (Fairlawn, NJ). SKOV-3 (Human Caucasian Ovarian Adenocarcinoma)[46], ES2 (Human Ovarian Clear Cell Carcinoma, a distinct histopathologic subtype of epithelial ovarian cancer)[46, 47], cell lines were purchased from American Type Culture Collection (Manassas, VA). Human Umbilical Vein Endothelial Cells (HUVEC)[48] cells and endothelial growth medium 2 were purchased from PromoCell (Heidelberg, Germany). Cells were cultured as per the manufacturer instructions and all experiments were performed between passages 2 and 6. CIM-Plates 16 for the migration assay were obtained from ACEA Biosciences Inc.(San Diego, CA), µ-Slide Angiogenesis ibiTreat were ordered form ibibi, LCC (Verona, WI). Matrigel for the tube formation assay was purchased from BD

Biosciences (San Jose, CA). Cleaved Caspase-3 Rabbit antibody was purchased form Cell Signaling Technology (Danvers MA). CD31 Rabbit polyclonal antibody was purchased from Abcam Inc. (Cambridge MA). Cy3-AffiniPure Donkey Anti-Rabbit IgG (H+L) antibody was purchased form Jackson Immune Research (West Grove, PA). Cell culture reagents, Fibronectin (Human Natural Corning) and disposables were purchased from VWR (Radnor, PA), Thermo Scientific (Fairlawn, NJ), or PromoCell (Heidelberg, Germany). CellTiter-Blue® Cell Viability Assay kit was obtained from Promega Inc. (Madison, WI). All other materials and reagents were of analytical grade and were obtained from Sigma-Aldrich Inc (Milwaukee, WI) or Thermo Scientific (Fairlawn, NJ).

2.2. Methods

2.2.1. Synthesis and characterization of PEG-p(Asp-Hyd-LEV-PTX) or PEG-p(Asp-Hyd-LEV-RAP)

The schematic for the synthesis is presented in Fig. 2. Fuchs-Farthing method[49] is followed to synthesize the β-benzyl-L-aspartate *N*-carboxyanhydride (BLA-NCA) (1). β-benzyl L-aspartate (25 g, 112 mmole) is dried under vacuum for 3 h and is mixed with 0.3 equivalent of triphosgene (10 g, 33.6 mmol) and the mixture is dissolved in 120 mL anhydrous THF and the reaction is run at 40 ^{o}C for 24 h under Argon atmosphere. Upon completion of the reaction, the solution becomes clear (indicative of BLA-NCA formation) and 300 mL of hexane is added to precipitate BLA-NCA (1) which is then purified by recrystallization from THF and hexane.

PEG-PBLA is synthesized using previously described methods[39, 40, 50, 51]. The BLA-NCA (1) (1.7 g, 6.82 mmol) is polymerized by ring opening initiated by the terminal primary amine group of PEG-NH_2 (2) (2.0 g, 0.16 mmol). The reaction is performed in anhydrous DMSO (40 mL) under argon at 45 ^{o}C for 48 h. The resulting PEG-PBLA (3) is precipitated using diethyl ether and freeze dried from benzene. The next step in the synthesis is the preparation of PEG-p(Asp-Hyd) (PEG-HYD) (4) by aminolysis reaction [41, 52-54]. The reaction is carried out on PEG-PBLA (1.0 g, 0.05 mmol) by dissolving it in anhydrous N,N-dimethylformamide (DMF) (20 mL). Anhydrous hydrazine (1.2 eq with respect to benzyl groups) is added to the polymer solution and the reaction is carried out at 40 ^{o}C, under argon for 12 h. The resulting PEG-HYD is precipitated in diethyl ether and freeze dried from benzene (4). The third step of the reaction introduces the linker, levulinic acid (LEV), to the polymer backbone for subsequent drug attachment[41, 42]. The hydrazine groups on the PEG-HYD (750 mg , 0.046 mmol) are reacted with the ketone group on the LEV (1.2 eq with respect to hydrazide group) in 15 mL of anhydrous DMSO to form PEG-p(Asp-Hyd-LEV) (PEG-LEV) (5). The reaction is carried out at 45 ^{o}C for 48 h, followed by precipitation of the PEG-LEV from diethyl ether. Post precipitation the PEG-LEV is dissolved and dialyzed in DMF for purification, precipitated in diethyl ether and freeze dried from benzene. PTX or RAP conjugation is the final step in this reaction scheme. The reaction is carried out by dissolving PTX (1.57 g, 1.84. mmol) or RAP (2.00 g, 2.19 mmol) with PEG-LEV (1.00 g, LEV = 1.84 mmol) in a co-solvent system consisting of dichloromethane (DCM): DMF (3:1) (30 mL) along with N,N'-diisopropylcarbodiimide (DIC; 0.29 g, 2.30 mmol) and 4-dimethylaminopyridine (DMAP; 0.12 g, 0.95 mmol). The reaction is allowed to proceed at 25 ^{o}C for 96 h and the resulting PEG-p(Asp-Hyd-LEV-PTX) (PEG-LEV-PTX)[41, 42] or PEG-p(Asp-Hyd-LEV-RAP) (PEG-

LEV-RAP) (6) is collected by evaporating the DCM. The residue is diluted in DMF and dialyzed against 1.0 L DMF (DMF is changed 3 times) using regenerated cellulose (MWCO: 6-8000 g/mol). The polymer is precipitation in diethyl ether and freeze dried from benzene. For each step of the reaction the structure is confirmed by ^{1}H NMR (400MHz, DMSO-d6), FT-IR and the molecular weight is assessed using gel permeation chromatography (GPC). The amount of drug conjugated is quantified by ^{1}H NMR (400MHz, DMSO-d6), and Reversed-phase HPLC (RP-HPLC).

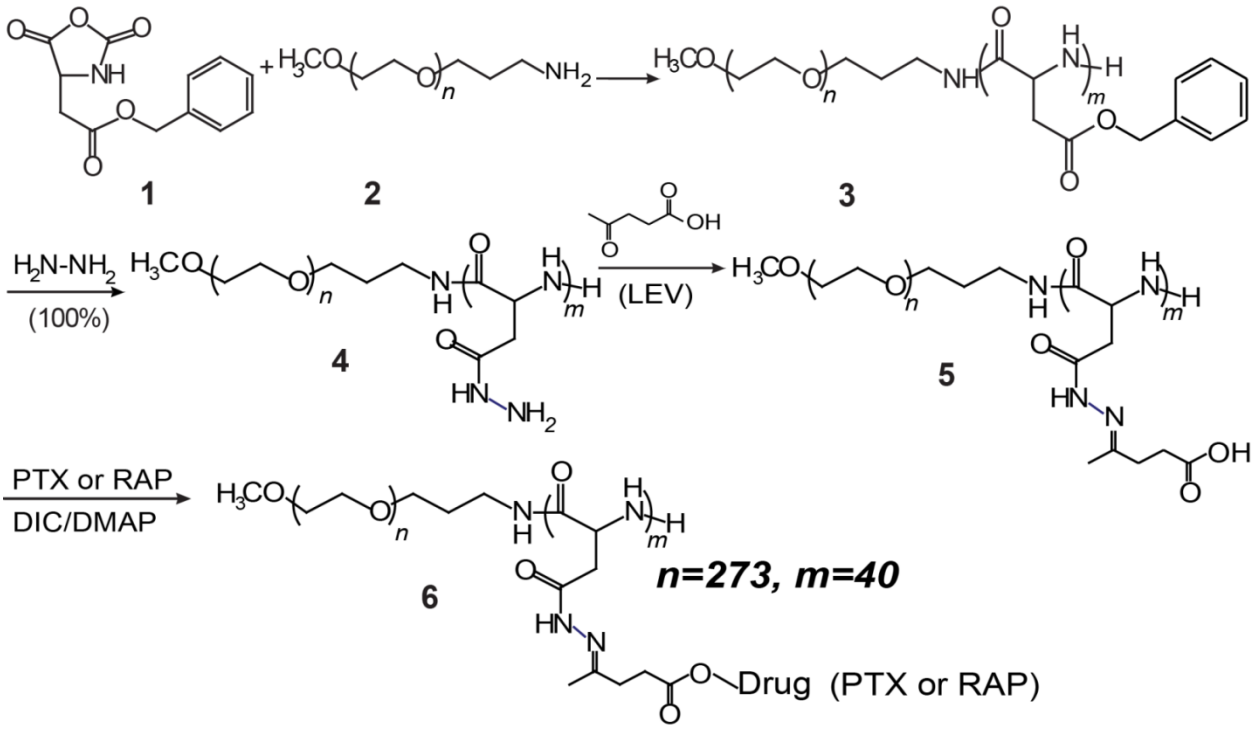

Fig. 2. Synthesis schematic for PEG-LEV-PTX[41, 42] or PEG-LEV-RAP

NMR measurements are performed on a DPX-400 NMR Spectrometer (Bruker Corp. Billerica, MA) at 400 MHz normal proton frequencies. The sample temperature is maintained at 80 ^{o}C for the duration of the measurement. Acquisition parameters are adjusted on a case-by-case basis to provide adequate signal-to-noise and spectral resolution. All ^{1}H spectra are referenced with respect to DMSO at 2.5 ppm. FT-IR measurements are performed on Nicolet iS5 Mid-Infrared FT-IR spectrometer equipped with iD5 Diamond ATR for Nicolet iS5 (Thermo Scientific. Waltham, MA)

Gel permeation chromatography (GPC) analysis is performed for each of the synthesized polymers to evaluate the weight average molecular weight (M_w), the number average molecular weight (M_n), polydispersity index (PDI), Hydrodynamic Radius (R_h), intrinsic viscosity [η], and Mark-Houwinks constant α. The GPC measurements are carried out using a Viscotek system equipped with Viscotek GPC Max VE 2001 solvent sample module, column oven 90-225 revH, Viscotek VE 3500 RI detector, and Viscotek 270 Dual Detectors (light scattering operating and viscometer detectors) (Malvern Instruments Inc., UK). Tosho TSKgel G4000SW column (13 µm, 450 Å silica, 7.5 mm ID x 30 cm) (Tosoh Bioscience LLC, King of Prussia, PA) with DMF

stabilized with 10 mM LiBr as the eluting solvent at a flow rate of 1 mL/min is used. The column is maintained at 30 °C for the duration of analysis. Polymers are solubilized in DMF at concentrations of 20 mg/mL and filtered through a 0.2 µm filter prior to injecting 100 µL for analysis. Mw, Mn, PDI, [η] and α are computed using a triple detection method with a narrow polymethylmethacrylate (PMMA) standard (65,000 Da, PDI at 1.10, [η] of 0.245 dL/g and dn/dc of 0.057mL/g; Agilent Technologies., Santa Clara, CA). All measurements are performed in triplicate. The results are compiled using OmniSEC Software (Malvern Instruments Inc., UK)

RP-HPLC is performed on a Shimadzu prominence HPLC system (Shimadzu, JP), equipped with a LC-20AT pump, SIL-20AC HT autosampler, CTO-20AC column oven, and a SPD-M20A diode array detector. A Zorbax SB-C8 Rapid Resolution cartridge (4.6×75mm, 3.5 micron) (Agilent Technologies, Santa Clara, CA) is used to quantify the amount of conjugated PTX or RAP. Run conditions include a mobile phase of Acetonitrile (ACN):Water (47:53) with 1% methanol and 0.1% H_3PO_4 run in isocratic mode at 1mL/min. Injection volume of 10 µL is used and the column temperature is maintained at 40 ^oC with a run time of 8 min. PTX and RAP are detected by UV at 3.3 min and 5.6 min respectively at wavelengths of 227 nm and 279 nm respectively. To quantify the amount of conjugated drug, PEG-LEV-PTX or PEG-LEV-RAP, is incubated in 550 µL double distilled (DD) H_2O, 400 µL ACN and 50 µL of 6 N Hydrochloric acid (PTX) or 5 N acetic acid (RAP) to ensure complete hydrolysis of the hydrazone bond and the release of PTX or RAP from the polymer backbone. Post-incubation, the samples are centrifuged at 10,000 rpm for 3 min and filtered using a 0.45 µm nylon filter and injected into the column for analysis.

2.2.2. Preparation and characterization of PTX micelles (PTX-M), RAP micelles (RAP-M), and PTX:RAP 1:1 molar ratio mixed micelles (MIX-M)

To prepare individual micelles, PTX-M or RAP-M; PEG-LEV-PTX or PEG-LEV-RAP polymer at 10 mg corresponding to, 4.4 µmol PTX or 4.3 µmol RAP respectively is dissolved in 1 mL of ACN and the resulting solution is placed in a 10 mL round bottom flask. The ACN is fully evaporated under vacuum (200 mbar) at 40 ^oC for 10 min. The formed film is rehydrated in 1 mL 10 mM phosphate buffer (pH 7.4) and the final micellar solution is filtered using a 0.45 µm nylon filter. The MIX-M are prepared similarly with 10 mg total of the polymer with 5 mg polymer corresponding to 2.4 µmol PTX and 5 mg polymer corresponding to, 2.2 µmol RAP to achieve a 1:1 molar ratio of the two drugs. PTX-M, RAP-M or MIX-M are assessed for loading by RP-HPLC (section 2.2.1), size by dynamic light scattering (DLS) and drug release by dialysis.

The hydrodynamic diameters of the micelles are calculated using a ZETASIZER Nano-ZS (Malvern Instruments Inc., UK) equipped with He-Ne laser (4mW, 633 nm) light source and scattering angle of 173^o collection configuration to determine micelles mean diameters by this DLS technique. All measurements are done in triplicate, and the data is presented as mean volume weighted diameters ± SD along with the corresponding polydispersity index (PDI).

The prepared micelles are imaged with Transmission Electron Microscopy (TEM). Samples are prepared by placing 3 µL of the micellar solution onto the copper grid coated with carbon. After removing the excess solution using a filter paper, the grid is left to dry for 10 min. The samples are examined at 120 kV on FEI Tecnai Spirit TEM system. Images are acquired as 2048x2048

pixel, 16-bit gray scale files using the FEI's TEM Imaging & Analysis (TIA) interface on an Eagle 2K CCD multi scan camera.

In vitro PTX and/or RAP release from the PTX-M, RAP-M, or MIX-M is evaluated by dialysis of the micelles against 10 mM acetate (pH 5.5) or phosphate (pH 7.4) buffer. Freshly prepared 2.5 mL of each micelle are loaded into 3 mL dialysis cassettes with a MWCO of 20,000 Da. This MWCO ensures free diffusion of the unconjugated drugs and dissociated polymer molecules. The cassettes are placed in 2.5 L of the buffer solution, which is changed every 3 h to ensure sink conditions. Samples of 150 µL are withdrawn and replaced with equal volume of fresh buffer at 0, 0.5, 1, 2, 3, 6, 9, 12, and 24 h. The samples are incubated in 400 µL ACN and 50 µL of 6 N Hydrochloric acid (PTX) or 5 N acetic acid (RAP) to ensure complete release of PTX and RAP from the polymer backbone prior to analysis by RP-HPLC. Data from three replicates is presented as mean percent (%) drug release ± SD. The data is further analyzed by curve fitting into a one phase exponential association using GraphPad Prism version 6.07 for Windows, GraphPad Software, La Jolla California, USA. Based on the curve fitting, a half-life for the association ($t_{1/2}$) and goodness of fit values (r^2) for the average of the three replicates is presented.

2.2.3. In vitro cell viability and combination index analysis studies in SKOV-3, ES2, and HUVEC cells

Cell viability in the presence of PTX-M, R AP-M, and MIX-M is assessed in two ovarian cancer cell lines (SKOV-3 and ES2) and an endothelial cell line (HUVEC). All cells are seeded in 96 well plates at 5000 cells/well and are allowed to attach for 12 h (cancer cells) or 24 h (HUVEC). Post attachment cells are treated with 10 mM phosphate buffer (control), PEG-LEV directly dissolve in PBS at 100 nM (vehicle control) , PTX-M, RAP-M, or MIX-M (section 2.2) at dose ranges of 10 pM -10 µM (corresponding to PTX and/or RAP). Treated and untreated cells are incubated for 72 h (cancer cells) or 48 h (HUVEC) at 37 ^{o}C in 5% CO_2 atmosphere. Additionally the effect of PTX and/or RAP in DMSO on the viability of the same cells is assessed. PTX concentration ranges of 5 pM-500 µM while for RAP ranges of 5 nM-500 µM. Post-treatment cell treated with 20 µL/well Cell Titer Blue® and allowing the plates to incubate for 1.5 h at 37 ^{o}C. Post-incubation the cell viability is assessed by fluorescence at $560_{EX}/590_{EM}$. All experiments are performed in quadruplicate and data is presented as mean drug concentration at 50% growth inhibition (IC_{50}) ± SD. The IC_{50} values are calculated using the linearized median-effect plot with the CompuSyn software (Version 1.0, ComboSyn Inc., U.S.)[55]. The same software is utilized to calculate the combination index (CI) values for the MIX-M combination. Based on the Chou and Talay median-effect principle, CI values of <1, 1, and >1 are indicative of synergy, additivity, and antagonism respectively[56]. The software calculates the fraction of cells affected (F_a) and correlates it with the CI, providing the ability to assess effects at various drug concentrations in the combination. The curve fitting of CI vs Fa for the average of four replicates is presented.

2.2.4. In vitro real-time migration and tube formation studies in HUVECs

HUVEC migration is assessed using the xCELLigence RTCA DP system (Roche Applied Sciences, Germany) which measures the change in electrical impedance (recorded as cell

index number) as cells migrate from the apical to the basolateral chamber in response to a chemoattractant. To assess the migration, CIM-Plates 16 are coated with 20 µg/mL of fibronectin and allowed to incubate for 1 h. HUVEC cells are prepared for the experiment by starvation in serum free media for 4 h. After which, cells are detached and seeded onto the fibronectin coated CIM-Plates 16 at 15,000 cells/well. Cells are treated with PTX-M (0.2 nM), RAP-M micelles (0.2 nM), MIX-M (0.2 nM equivalent with PTX at 0.1 nM and RAP at 0.1 nM) or no treatment (control). Migration from apical to the basolateral chamber containing complete growth medium is monitored every 10 min for 48 h. Data for quadruplicate replicates is presented as mean cell index number ± SD. Statistical analysis using one-way ANOVA with Tukey's post-test was conducted using GraphPad Prism version 6.07 for Windows, GraphPad Software, La Jolla California, USA.

HUVEC endothelial tube formation assay was performed using matrigel coated µSlide Angiogenesis, ibiTreat plates. Matrigel is thawed overnight in an ice bath (4 ^{o}C) and is then used to coat the wells at 50 µL/well. Post coating, the wells are incubated at 37 ^{o}C for 60 minutes to allow for gelation. HUVECs are seeded at 20,000 cells/well and allowed to incubate at 37 ^{o}C for 18 h and cells are treated with PTX-M (0.2 nM), RAP-M micelles (0.2 nM) (C), MIX-M (0.2 nM equivalent with PTX at 0.1 nM and RAP at 0.1 nM) or no treatment (control) for 10 h. After the experiment, the total tube length and area are measured using NIH ImageJ analysis software. All experiments are performed in quadruplicate and representative images are presented.

2.2.5. In vivo acute toxicity study in healthy mice

Female nu/nu athymic mice 6-to-8 weeks old with an average weight of 20 to 22 g (Frederick National Laboratory for Cancer Research, Frederick, MD) are utilized to determine the acute toxicity of PTX-M, RAP-M and MIX-M. Mice are separated into 5 groups with 5 mice per group (n = 25). The groups include control (normal saline), PEG-LEV, PTX-M, RAP-M or MIX-M. Mice injected via tail vein at volumes corresponding to 80 -120 µL adjusted to the weight of each mice to ensure identical doses. The dose of the polymer or polymer and drug conjugate for PEG-LEV, PTX-M, RAP-M or MIX-M are150 mg/kg, (corresponding to PTX or RAP or both drugs at 60 mg/kg). The dose of 150 mg/kg (polymer-drug conjugate) was highest dose possible based on polymer solubility. For the MIX-M, the dose of RAP and PTX were 30 mg/kg each (total drug dose of 60 mg/kg). The mice are injected on days 0, 4, and 8 and monitored for signs of acute toxicity, which include, changes in behavior, weight loss > 15%, or death over 21 days. Data is presented as mean percent (%) normalized body weight ± SD. All animal work is performed in compliance with NIH guidelines and Oregon State University IACUC Policy for End-Stage Illness and Pre-emptive Euthanasia, based on Humane Endpoints Guidelines.

2.2.6. In vivo efficacy studies in ES2 murine xenograft model

Female nu/nu athymic mice 6-to-8 weeks old with an average weight of 20 to 22 g (Frederick National Laboratory for Cancer Research, Frederick, MD) are implanted subcutaneously on the flank with ES2 at $1x10^6$ cells to generate an ovarian cancer xenograft model. When the primary tumor volume reaches 150 to 200 mm^3 (approximately 7-14 days), animals are randomized into 5 groups (n = 25; 5/group). Each group is treated by lateral tail vain injections with the

vehicle/control (normal saline), PEG-LEV, PTX M, RAP-M, or MIX-M. The volume of injection ranges between 80-120 µL as it is adjusted to the weight of each mouse to ensure identical doses. The PEG-LEV is dosed at 50 mg/kg, while the micelles are dosed at 20 mg/kg of individual drugs or 10 mg/kg of each drug in the MIX-M (total amount of polymer injected 50 mg/kg). Mice are injected on days 0, 4, and 8 and tumor growth is assessed using a vernier caliper every 3 to 4 days. Tumor volumes are estimated by π/6 x length x width^2. At the end of the experiments, % T/C values, (Δtumor volume$_{treated}$/Δtumor volume$_{control}$ x 100) are calculated, where Δtumor volume represents the mean tumor volume on the test day minus the mean tumor volume at the start of the experiment. Mice are monitored for acute toxicity as defined by weight loss of ≥15% versus control, remarkable changes in general appearance, or death. Mice are euthanized at 21 days or when tumor volume reaches 3000 mm^3. Tumor tissue is collected and samples are fixed in 4% paraformaldehyde overnight and embedded in paraffin blocks. Immunohistochemistry (IHC) studies using 5 µm section are performed as previously described.[57] Anti-CD31 and anti-Cleaved Caspase-3 are used as primary antibodies to detect the density of the tumor-associated microvessels (angiogenesis) and apoptotic cells respectively. Goat anti-rabbit CY3 is used as the secondary antibody (red). Nuclei are counterstained with DAPI (blue). All images are captured using a Zeiss AXIO ImagerZ1 with a digital AxioCam HRm and processed using AxioVision 4.7 (Carl Zeiss Microscopy, LLC) and Adobe Photoshop CS5 software. Cell quantifications are performed using NIH ImageJ software and multiple IHC fields on each slide from all groups are randomly chosen and at least 15 fields per group are counted. For apoptosis evaluation, the number of apoptotic cells positive to cleaved caspase 3 staining are counted in a minimum of 4 random fields (0.55 mm^2, 20X magnification) per tumor section for 4 different tumors. The apoptotic index (%) is quantified using apoptotic cell number/total cell number x 100. For angiogenesis evaluation, the CD31 positive area percent (%) is calculated as CD31 positive area/total measured area x 100. At least 4 random fields (0.55 mm^2, 20X magnification) per tumor section for 4 tumors are quantified to measure the CD31 positive area and calculate the % area as described above.

All animal work is performed in compliance with NIH guidelines and Oregon State University IACUC Policy for End-Stage Illness and Pre-emptive Euthanasia, based on Humane Endpoints Guidelines. Statistical analysis for tumor volume is performed using one-way ANOVA at 5% significance level with Tukey's Multiple Comparison post-test with groups compared at 5% significance level. Significance for immunohistochemistry is determined using one-way ANOVA at 5% significance level with Dunnett's Multiple Comparison post-test with groups compared to control at 5% significance level. All statistical analyses are performed using GraphPad Prism software version 6.07 for Windows, GraphPad Software, San Diego, California USA.

3. Results & Discussion

3.1. Synthesis and characterization of PEG-p(Asp-Hyd-LEV-PTX) or PEG-p(Asp-Hyd-LEV-RAP)

The synthetic scheme for polymer-drug conjugations with PTX or RAP is depicted in Fig. 2. The structure of PEG-PBLA (3) is confirmed by ^{1}H NMR and the number of β-benzyl-L-aspartate units on PEG-PBLA is 40 (Fig.S1.) The polymerization of the PEG-PBLA is also confirmed by

FT-IR spectroscopy which indicated the disappearance of two peaks corresponding to the BLA-NCA (1850 and 1790 cm^{-1})(Fig.S4)[58]. The M_n and the PDI of PEG-PBLA were 20, 200 g/mol and 1.19, respectively. PEG-HYD (4) is synthesized by an ester-amide exchange reaction, and its structure is confirmed by ^{1}H NMR and FT-IR (Fig.S2 & Fig.S4 respectively). PTX and RAP lack an aldehyde or ketone functional group for hydrazone chemistry. To address this issue we previously developed a polymer backbone that contains an aliphatic linker, LEV as a spacer group on PEG-HYD, to conjugate compounds that contain primary alcohol via ester bond. [41, 42] PEG-LEV (5) is synthesized by a hydrazone bond formation between the hydrazide groups on PEG-p(Asp-Hyd) (4) and the ketone group on LEV[41, 42]. The number of LEV present in the PEG-LEV (5) is 40, corresponding to a 100% substitution and is confirmed by ^{1}H NMR (Fig.S3) and the M_n(NMR & GPC), M_w, and PDI of the PEG-LEV are presented in Table 1. PEG-LEV-PTX (6) is synthesized by conjugation of PTX via an ester bond on PEG-LEV using a previously described method[41, 42]. The structure of PEG-LEV-PTX polymer is confirmed by ^{1}H NMR[41, 42]. The number of PTX molecules present in PEG-LEV-PTX (6) is 15 as calculated from ^{1}H NMR [41, 42] and GPC data (Table 1), corresponding to a 37.5% degree of drug substitution. The M_n(NMR & GPC), M_w, and PDI for the PEG-LEV-PTX are also presented in Table 1. RAP is conjugated to the PEG-LEV polymer utilizing the same method as PTX conjugation. The structure of PEG-LEV-RAP is also confirmed by ^{1}H-NMR (Fig .3), FT-IR (Fig.S4) and GPC (Table 1). The number of RAP molecules present in PEG-LEV-RAP is 16 and is calculated from the peak ratio of the methylene protons of PEG (-OCH2CH2- : δ 3.5 ppm) (resonance b) to RAP methyl protons (3H -CH3- : δ 1.11 ppm) (resonance 45) (Fig.3), corresponding to a 40.0% degree of drug substitution. Ester prodrugs for RAP such as everolimus, temsirolimus, and deforolimus involves its C-40-OH position[59] (Fig.3) however the position of RAP conjunction in PEG-LEV-RAP was not confirmed by ^{1}H-NMR. The M_n (NMR & GPC), M_w, and PDI for the PEG-LEV-RAP are presented in Table 1. For the three polymers, the measured molecular weights from ^{1}H NMR and GPC are in good agreement and based on the TEM images (Fig.S5.) and the calculated PDI values all of the polymers indicate a monodispersed population.

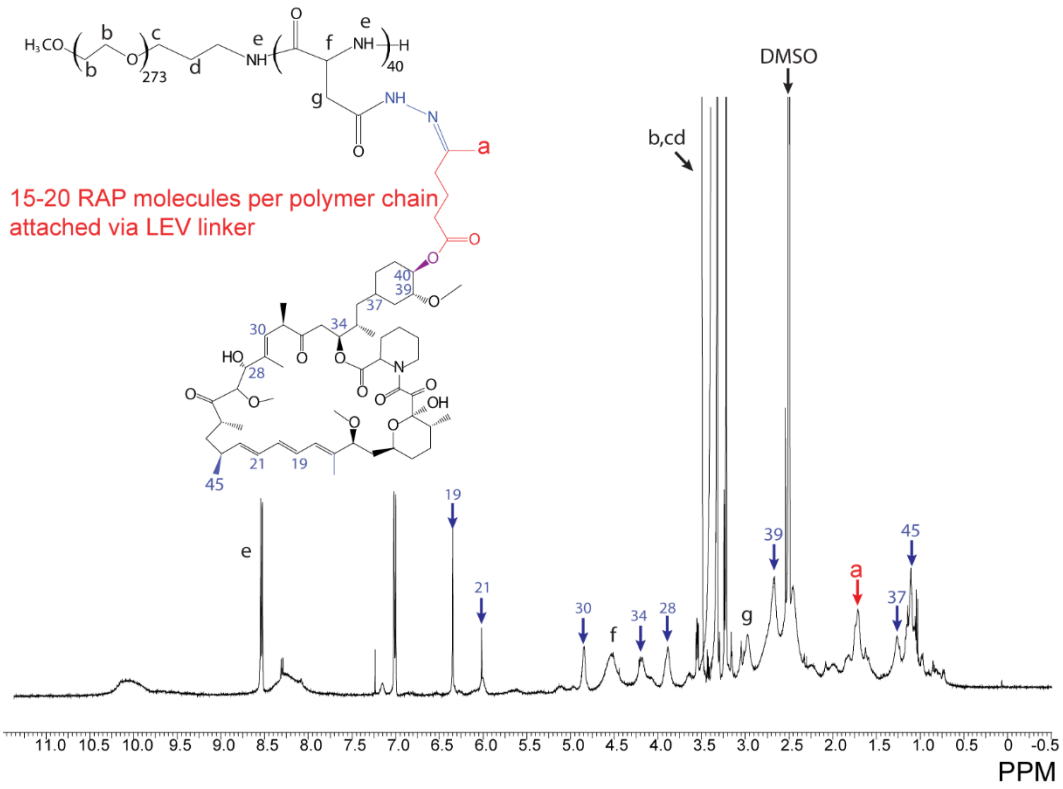

Fig. 3. ^{1}H NMR spectra of PEG-LEV-RAP (6). NMR measurements are performed on a DPX-400 NMR Spectrometer at 400 MHz in DMSO-d6 and at 80 ^{o}C.

RP-HPLC measurements are used to confirm the absence of un-reacted PTX and RAP. RP-HPLC analysis of the PEG-LEV-PTX resulted in a retention time of 1.30 min as detected by UV at its λ_{max} of 227 nm as a single peak while free PTX elutes at 3.3 min. Similarly, PEG-LEV-RAP elutes at 2.00 min as detected at its λ_{max} of 279 nm as a single peak, while free RAP elutes at 5.6 min. Upon purification of the PEG-LEV-PTX or PEG-LEV-RAP no free PTX or RAP is detected. Based on RP-HPLC analysis the amount of the PTX per polymer is 0.38 g per 1 g of PEG-LEV-PTX, while the amount of RAP per polymer is 0.39 g per 1 g of PEG-LEV-RAP.

Intrinsic viscosity [η] is specific property for a polymer that measures the polymer's ability to increase the viscosity of a solvent, and it is used for determining the polymer size, molecular weight, and topology[60]. The [η] is related to the hydrodynamic radius, R_h, by the Flory-Fox expression[61]. Also [η] is related to molecular weight by the Mark-Houwink−Sakurada equation given as $[\eta] = KM^{\alpha}$, where M is the molecular weight while K and α are constants for a given polymer, solvent, and temperature. The α value is strongly associated with the polymer rigidity and shape, for compact/spherical chains α < 0.5, for random-coil/flexible chain α usually lies in the range of 0.5-0.8, while α > 0.8 for rigid-rod/stiff chain [62]. The [η], R_h and α values for PEG-LEV, PEG-LEV-PTX and PEG-LEV-RAP are presented in Table 1. The [η] for the three polymers has different values inductive of different chemical and physical compositions resulting in different behaviors in the solvent system. PEG-LEV forms rigid chains (α of 1.9) with an R_h of 6.6 nm. PEG-LEV-PTX polymer chains exist as random /flexible chains (α of 0.5) with an R_h of 4.6 nm, while PEG-LEV-RAP forms compact spheres (α of 0.3) with an R_h of 4.7 nm. These

data clearly indicate that the conjugations of the PTX or RAP to the PEG-LEV backbone results in the formation of two new polymer-conjugates that behave differently and form different secondary structures in a solvent system.

Table 1: Characterization of the synthesized polymers

Polymer	M_n(NMR) (g/mol)[a]	M_w (g/mol)[b]	M_n (g/mol)[b]	PDI (M_w/M_n)[b]	# of drug molecules[a,b,c]	[η] (dl/g)[b]	R_h (nm)[b]	Mark-Houwink Constant[b] α
PEG-LEV	21,080	21,798	19,381	1.13	------	0.1558	6.6	1.9
PEG-LEV-PTX	33,620	35,081	30,042	1.17	15	0.1793	4.6	0.5
PEG-LEV-RAP	35,432	36,353	28,568	1.27	16	0.2154	4.7	0.3

[a] Determined by ^{1}H NMR

[b] Determined by GPC, Triple detection method, calibration was established with narrow PMMA standard, DMF with 10 mM LiBr

[c] Determined by: $(\mathrm{Mw\ (PEG-LEV-Drug)} - \mathrm{Mw\ (PEG-LEV)}) \,/\, \mathrm{Mw\ (drug)}$

3.2. Preparation and characterization of PTX-M, RAP-M, and MIX-M

RP-HPLC indicates that PTX-M and RAP-M has 4.4 µmol of PTX and 4.3 µmol of RAP per 1 mL of micellar solution. In the case of the MIX-M, 2.4 µmol PTX and 2.2 µmol of RAP are present in 1 mL of micellar solution. DLS is used to determine the particle size of freshly prepared PTX-M, RAP-M, and MIX-M. All micelles exhibited monodisperse population. The size of PTX-M, RAP-M, and MIX-M are 41.9 $\pm$ 0.6 nm (PDI = 0.112 ± 0.005), 90.1 $\pm$ 2.1 nm (PDI = 0.128 ± 0.023), and 102.3 $\pm$ 3.5 nm (PDI = 0.138 ± 0.009) respectively. The spherical shape and monodispersity of the micelles are further confirmed by TEM measurements (Fig.S5). The larger size of the RAP-M compared to PTX-M for the same polymer backbone is possibly due to differences in the packing of the micelles core and this speculation is supported by the Mark-Houwink Constants α values (Table 1) that PEG-LEV-PTX and PEG-LEV-RAP polymers chains exist in different conformations in polar solvents such as DMF and water. This effect has been also documented elsewhere where changes in the hydrophobicity of the core can have significant impact on micelle packing, size, and stability[63]. The sizes for MIX-M and RAP-M are similar, indicating that the RAP packing has a greater impact on the overall size of the micelle.

Release of the conjugated drug(s) from the micelles over 24 h was performed under sink conditions at pH 7.4 (mimicking physiological pH), and pH 5.5 (mimicking acidic conditions associated with the endosomal/lysosomal pathway of cells)[52-54, 64]. The release data for the PTX-M, RAP-M, and MIX-M along with their respective fitted curves is presented in (Fig.4). As

seen in the drug release profile, the release of the drug from the polymer backbone is greater at pH 5.5 as compare to pH 7.4. This is expected as the hydrazone linker, LEV, is cleaved from the polymer backbone at acidic pH[42, 52-54, 64]. The drugs release profile for the individual and mixed micelles did not reach 100% within 24 h, suggesting that some of the hydrazone bonds have not been cleaved during the experimental time frame. Our findings are in agreement with previous studies[42, 43]. Nonlinear curve fitting using a one phase exponential association indicates that a good fit is achieved at pH 5.5 but not at pH 7.4. At pH 5.5 the $t_{1/2}$ and r^2 values for the fitting for PTX-M are 6.85 h and 0.9782 respectively, while at pH 7.4, no $t_{1/2}$ could be calculated and with r^2 value of 0.8924 (Fig. 4A). As the major step in the drug release is the cleavage of the linker from the polymer backbone, it is not surprising that at pH 7.4 minimal release occurs, and therefore, curve fitting is ambiguous for PTX in PTX-M. Interestingly, RAP-M release data at both pHs could be curve fitted using the one phase exponential association. The $t_{1/2}$ and r^2 values for RAP-M at pH 5.5 are 2.34 h and 0.9173, while at pH 7.4 it is 2.60 h and 0.9554 respectively. However, as seen in Fig.4B the rate of RAP release from RAP-M is much slower, with only ~30% of the RAP released in 24 h at pH 7.4 versus ~60% release at pH 5.5. In the case of the MIX-M (Fig. 4C), the release patterns for both drugs at both pHs changes indicating that the packing of the drug conjugated polymers is different in these micelles. The $t_{1/2}$ and r^2 values for PTX in MIX-M at pH 5.5 are 0.87 h and 0.9484, respectively, while for RAP these values are 0.92 h and 0.9121 respectively. At pH 7.4, the $t_{1/2}$ and r^2 values for PTX in MIX-M are 0.31 h and 0.5685 respectively, while for RAP these values are 1.12 h and 0.7420. This data shows the release profile for PTX and RAP from MIX-M is also dependent on the pH and it is higher at pH 5.5. Interestingly, the release profile of PTX and RAP are nearly identical pH 7.4 but show slight differences in the extent of release at pH 5.5 (Fig. 4C). The release profile of PTX and RAP from individual and MIX-M is not the same and it is clearly depended on the composition and the core properties of the polymeric micelle.

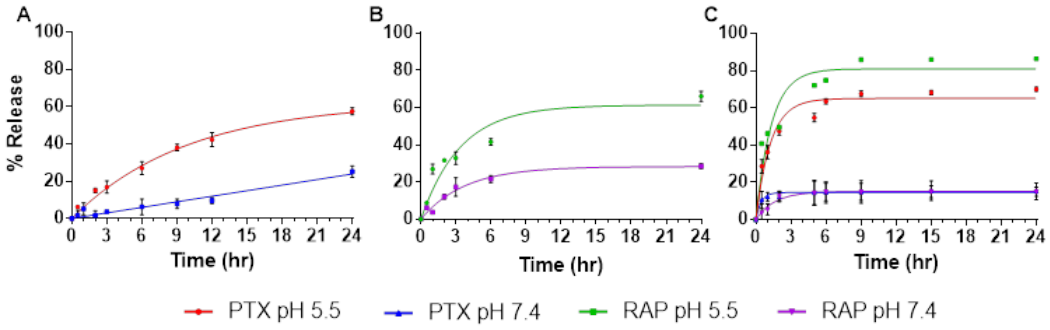

Fig.4. Release of PTX and/or RAP from PTX-M (A), RAP-M (B), and MIX-M (C) at pH 5.5 & 7.4 under sink conditions (37 °C, n=3). The solid lines represent the nonlinear curve fitting of the data using a one phase exponential association.

3.3. In vitro cell viability and combination index analysis studies in SKOV-3, ES2, and HUVEC cells

Prior to the initiation of animal studies, cell-based viability studies were performed in two ovarian cancer lines (SKOV-3 and ES2) and in an endothelial cell line (HUVEC). The IC_{50} values for each of the micelles in all three cell lines are presented in Fig.5.(A-C) and the IC_{50} values for the

free drugs and their combination are presented in Fig.S6. The IC_{50} of PTX-M and RAP-M in all the cell lines are in nM range indicating the strong anti-proliferative effect of each of the drugs in their respective micelles. The IC_{50} of the MIX-M irrespective of the cell line, demonstrated greater potency than either of the individual micelles, further analysis to determine the nature and the degree of interaction was performed using CI analysis. The CI analysis (Fig. 5D) indicates that for all three cell lines the MIX-M containing PTX and RAP are synergistic (CI < 1) at all fractions of cells affected (Fa). Comparing the anti-proliferative effect of the free drug and micelles, PTX is slightly more potent than PTX-M in the SKOV-3 and HUVEC cell lines, while free RAP is significantly less potent than RAP-M in all three cell lines as indicated by the higher IC_{50}. We speculate the reason behind that is RAP-M increased the solubility of RAP significantly thereby producing a stronger inhibition on cell viability. CI analysis indicates that in all three cell lines at lower fractions affected the free drugs are synergistic but become antagonistic at higher fractions of cells affected (Fig.S6) unlike the MIX-M which remains synergistic at all fractions affected.

PTX is a mitotic inhibitor that stabilizes microtubules while RAP inhibits the activation of the mammalian Target of Rapamycin (mTOR)[59, 65, 66]. Thus, the dual mechanisms of actions of the two drugs, acting together, decrease the ability of the cell to overcome the cytotoxic effects. Our findings are in agreement with the findings of others who showed that RAP potentiates the cytotoxicity of taxanes in different cancer cell lines. Liu et al. showed that in two prostate cancer cell lines RAP acts synergistically with docetaxel by enhancing docetaxel-induced upregulation of caspase activity through cell cycle arrest in sub-G1 phase[67]. In another study, the effect of RAP and PTX combination on two ovarian cancer cell lines, SKOV-3 and A2780, is assessed and the two compounds act synergistically to inhibit cell proliferation, induce cell apoptosis, and down-regulate the expression of survivin[68]. The same combination of RAP and PTX when evaluated in endometrial cancer cells demonstrated similar findings with the PTX and RAP combination synergistically inhibiting cell proliferation and inducing cell apoptosis[69]. The anti-proliferative effect of PTX-M, RAP-M, and MIX-M against HUVEC cells is also in agreement with our previous work in which PTX and RAP loaded in PEG-*b*-PLA micelles inhibited HUVEC cell proliferation and their combination acts synergistically. In addition, others have demonstrated that both PTX and RAP individually inhibits the proliferation of HUVEC at nM concentrations[28, 29].

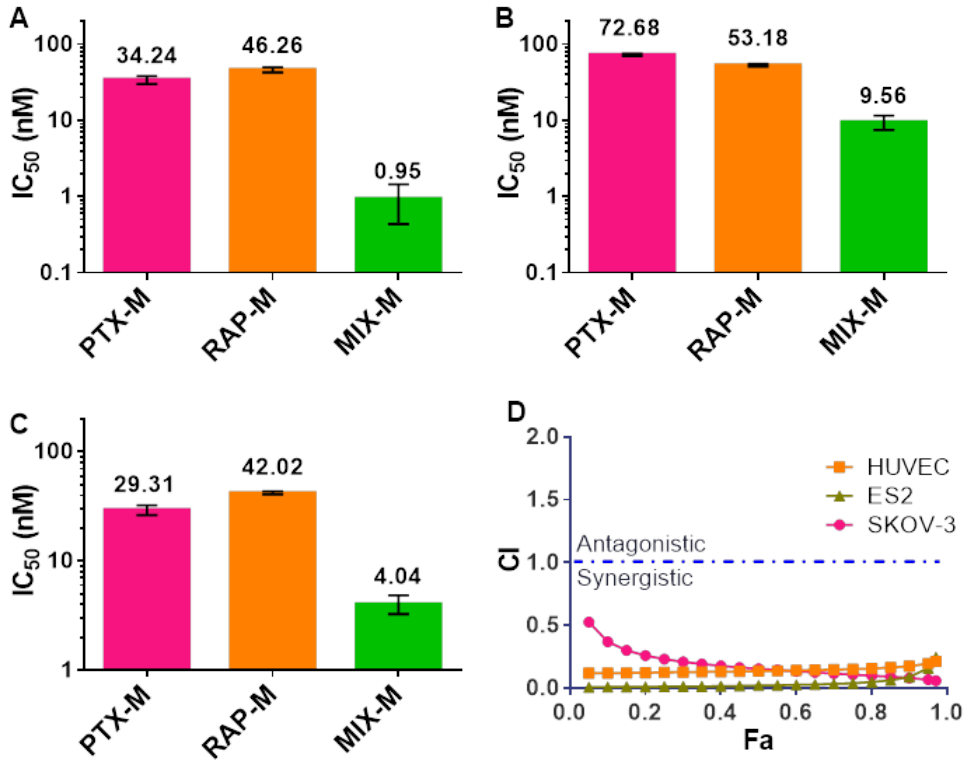

Fig. 5. IC_{50} values for PTX-M, RAP-M, and MIX-M in ES2 cells (A), SKOV-3 cells (B), and HUVEC (C); Fa vs CI plots for MIX-M in ES2 cells, SKOV-3 cells, and HUVEC (D). Error bars represent (Mean ± SD, n=4).

3.4. In vitro real-time migration and tube formation studies in HUVECs

As both, PTX and RAP, individually have the ability to inhibit the angiogenic cascade processes of proliferation, migration, and tube formation[22, 23, 33] in this study we wanted to assess the efficacy of these drugs in the individual and mixed micelles. Two aspects of angiogenesis processes, migration and tube formation, are assessed using HUVEC. The treatment groups in both experiments were HUVEC left untreated (control), treated with 0.2 nM of PTX, RAP in individual micelles or 0.1 nM of each in MIX-M. PTX-M and RAP-M concentrations selected for the studies were below the IC_{50} values in HUVEC of the micelles (Fig.5). This selection was based on earlier findings that PTX and RAP inhibit endothelial migration and tube formation at much lower doses than their IC_{50}[33, 70]. Data from the migration assay is presented in Fig. 6A. As seen in the data, the migration of HUVEC significantly decreased over 48 h as compared to control cells when treated with PTX-M, RAP-M, or MIX-M. No significant differences were noted in the migration upon comparing PTX-M, RAP-M, or MIX-M. Cell migration process is regulated through reorientation of centrosome in the intended direction of movement[71]. A change in microtubule plasticity can also alter the reorientation of the centrosome[71]. Based on these mechanisms, and our data, we postulate that PTX-M, RAP-M and MIX-M interfere with these processes and thereby inhibit cell migration.

In the tube formation assay, at 18 h, post-treatment images were obtained to ascertain the degree of tube formation. A representative set of these images is presented in Fig. 6B. As seen in the figure, control cells (I) have the highest degree of tube formation followed by PTX-M (II) or RAP-M (III), and then the MIX-M(IV). In the case of the MIX-M the tube formation seems to be highly disrupted again indicating that the conjugation of the drugs to the polymer backbone does not interfere with the anti-angiogenic activity of PTX and RAP and synergistic effects are not lost. Endothelial tube formation involves multiple steps such as attachment and migration prior to the tube formation process. Tube formation is initiated with attachment of endothelial cells on the basement matrix and then is followed by migration of these cells toward each other to eventually form tubes[72]. Our data has shown these process can be inhibited at concentrations well below the IC_{50} value of PTX-M and RAP-M and MIX-M (Fig. 6). It was reported that PTX and other taxanes cause cell cycle arrest in S phase or G1/S phase at lower concentrations, which is primarily responsible for inhibiting the tube formation process[70]. RAP and other mTOR inhibitors effect VEGF expression and block the endothelial transition to mesenchymal[29]. In MIX-M significant inhibition of HUVEC tube formation was observed presumably due to PTX and RAP acting on different pathways in the endothelial cells to produce a synergistic effect. This assumption is based on previous findings in which RAP has the ability to potentiate the effect of PTX and docetaxel through inhibition of cancer cell proliferation and induction of apoptosis[67, 69]. In addition, Mishra et al. showed that RAP produces antiangiogenic effects and acts synergistically with PTX to inhibit the angiogenic cascade processes of proliferation, migration, and tube formation[33]. These finding are further confirmed in our work in which we have shown that MIX-M affects angiogenesis by inhibiting HUVEC cells proliferation, migration, and tube formation (Figs. 5 and 6). Based on the cell viability, migration, and tube formation assays, the individual and mixed micelles offer the capability to use these conjugated micellar systems for targeting cancer cells or angiogenesis, thus, providing a versatile platform for various treatment options.

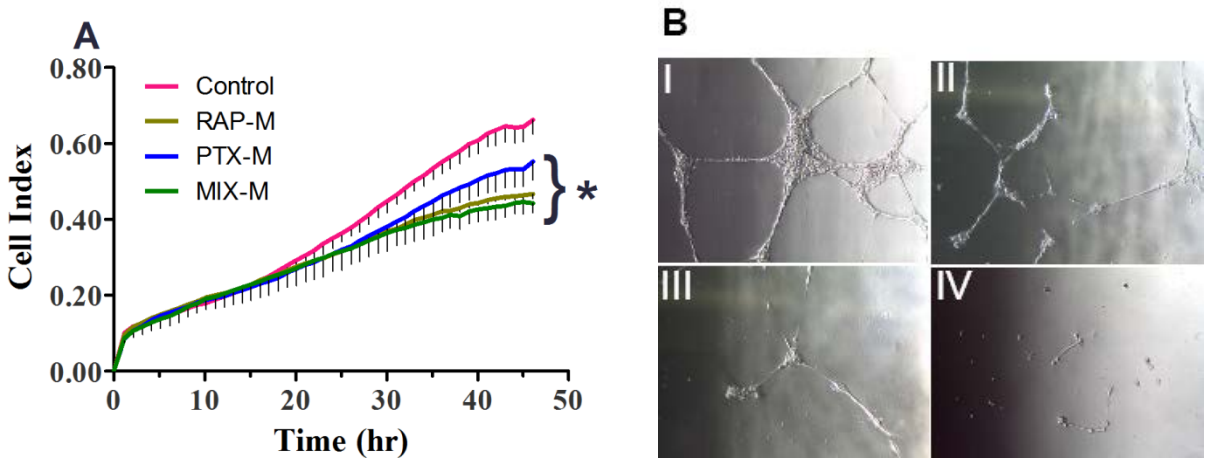

Fig. 6. Real-time cellular migration profile (RTCM) for HUVEC cells treated with: PTX-M 0.2 nM, RAP-M 0.2 nM, or MIX-M 0.2 nM (PTX 0.1 nM and RAP 0.1 nM), *Represents significant difference from untreated control. (Mean ± SD, n=4, α=0.05, 95% confidence intervals) (A); Tube formation assay:Control(I), PTX-M 0.2 nM (II), RAP-M micelles 0.2 nM (III), MIX-M 0.2 nM (PTX 0.1 nM and RAP 0.1 nM) (IV) (B). *Represents significant difference from control (saline)

(Mean ± SD, n=4). Significant differences between treatment group means were evaluated using one way ANOVA with Dunnett's Multiple Comparison Test (compare all columns vs. control) using a significant level (α) of 0.05. Analysis was performed with GraphPad Prism version 6.07 for Windows, GraphPad Software, San Diego, California USA,

3.5. In vivo acute toxicity study in healthy mice

Female nu/nu athymic mice are used to determine the acute toxicity due to treatment with the PEG-LEV, PTX-M, RAP-M, or MIX-M. Post-injection, mice were monitored for 21 days for changes in behavior, weight loss > 15 % and death. During the course of the study none of the mice treated exhibited any changes in behavior or died. Weight changes between the treatment and control (saline treated) groups is presented in Fig. 7. As seen in Fig. 7 none of the mice in the treatment groups are significantly different as compared to the control mice, indicating that treatment at such high concentrations with the drug(s) at (60 mg/kg/drug) have no adverse effects. Currently PTX is commercially available as Taxol® (Cremophor® EL-Ethanol formulation) and Abraxane™ (nanoparticles albumin-bound PTX). The MTD for PTX is highly dependent on the formulation. For example Taxol MTDs in mice range from 20-30 mg/kg/injection (i.v., every 2 days for 5 cycles)[73]. While the MTD for Abraxane in mice is 120 mg/kg (i.v., every fourth day for 3 cycles) [74]. Cynviloq™ (under clinical trials) is another formulation of PTX (PEG-*b*-PLA micelle physically loaded with PTX) has MTD of 50 mg/kg (i.v, every day for three days)[75, 76]. In comparison PTX-M showed no acute toxicity at a dose higher than Taxol® and comparable to Cynviloq™.

Currently there is no commercially available parenteral formulation for RAP. The MTD for RAP is 5 mg/kg/day I.P. injection for 5 consecutive days for 6 weeks where RAP is formulated in 5% DMSO, 5% Tween 80 in water[77]. Therefore RAP-M is a viable intravenous formulation for RAP and shows excellent safety. Interestingly, MIX-M showed non-additive acute toxicity in mice, indicating that such platform can be utilized for the co-delivery of PTX and RAP at clinically relevant concentrations. Shin et al. demonstrated the PTX and RAP co-delivered in PEG-*b*-PLA micelle at 60 mg/kg and 30 mg/kg respectively showed no acute toxicity in mice[45]. In comparison MIX-M was able to deliver PTX and RAP at 30 mg/kg each safely.

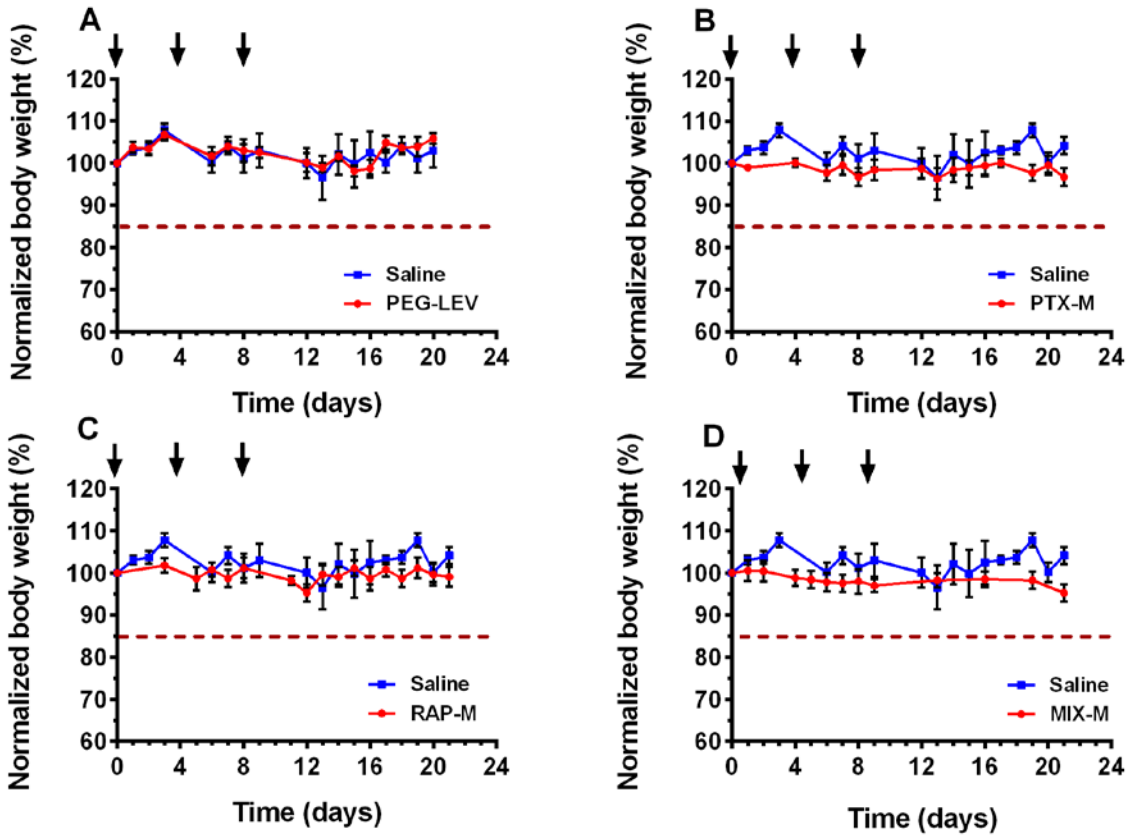

Fig. 7. Normalized body weight of mice over time after i.v. injection of PEG-LEV, PTX-M, RAP-M, and MIX-M on days 0, 4, and 8 as indicated by arrows. PEG-LEV (A), PTX-M at 60 mg/kg of PTX (B), RAP-M at 60 mg/kg of RAP (C), MIX-M at total drug 60 mg/kg (D) (30 mg/kg of PTX + 30 mg/kg of RAP) (n = 5/treatment, Mean ± SD). Mice were injected with saline as negative control. The horizontal dashed line in all figures represents loss in weight ≥ 15% body weight as an indication of toxicity.

3.6. In vivo efficacy studies in ES2 murine xenograft model

Individual and mixed micelle efficacy in treating ovarian cancer is evaluated in an ES2 xenograft model. Mice are treated at 20 mg/kg of individual drug or 10 mg/kg of each drug in MIX-M on day 0, 4, and 8, and tumor growth is assessed for 21 days post-treatment. As the dose-limiting toxicity DLT and MTD value could not be determined due to the limitation of the polymer-drug conjugate solubility (section 2.2.5). A lower dose and more frequent administration schedule of 3 doses every four days instead of one dose at MTD every 2-3 weeks is chosen to assess the cytotoxic and anti-angiogenic effect of the individual and mixed micelles. The lower dose with a greater frequency of administration mimics a MR dosing.

Tumor volumes (Fig. 8A), caspase-3 activity (Fig. 8B & 9A) and the density of blood vessels in the tumor tissue (Fig. 8C & 9B) are presented to demonstrate efficacy and mechanisms of action. The data presented in Fig 8A indicates that the PEG-LEV (polymer backbone) has no

effect on the tumor volume and it is not significantly different from the saline treated group, indicating that the polymer itself has no effect on tumor tissue. The tumor volumes for PTX-M and RAP-M, are smaller after 21 days as compared to saline or PEG-LEV, however no statistical difference is seen between the individual micelles and saline (Fig. 8A). MIX-M treated group produced significant reduction in tumor volume after 21 days as compared to the saline treated group. The highest reduction in tumor volume is seen in the MIX-M group, confirming the synergistic effects seen in the cell culture work.

To determine the effect of individual and mixed micelles on the ES2 xenograft, apoptosis induction and angiogenesis inhibition within the tumor tissue, are also evaluated and presented in Fig.8 & 9. Cleaved Caspase-3 assay is used to quantify the apoptotic activity as caspase-3 is a critical executioner of apoptosis and is either partially or fully responsible for the proteolytic cleavage of many key proteins within the cells[78]. Visually the IHC staining of the tumor tissue with the anti-Caspase-3 antibody (Fig. 9A) clearly indicates a higher density of apoptotic cells in the MIX-M group compared to the saline and PEG-LEV groups. Upon quantification, it is seen that only the MIX-M showed significant induction of apoptosis in the tumor tissue as compared to control (Fig. 8B & 9A). Thus, the tumor volume reduction with MIX-M is at least partially due to the induction of apoptosis that seems to occur due to the synergistic effects of PTX and RAP.

Interestingly, all micelles, PTX-M, RAP-M, and MIX-M, significantly inhibited angiogenesis formation within the tumor tissue as compared to saline (Fig. 8C & 9B). This inhibition is represented by the reduction in the of CD31 expression, which is a marker for endothelial cells (Fig. 9B). Further comparison between the micelle groups indicates that the MIX-M treated group has reduced the blood vessel density within the tumor region as compared to PTX-M and RAP-M (Fig 8C). Thus, in the case of MIX-M the tumor volume reduction is also driven by the inhibition of the angiogenesis, while in the case of the individual micelles, at these concentrations only angiogenesis inhibition occurs but no cytotoxic effects are seen. The ability of PTX and RAP to induce an antiangiogenic effect is well documented in the literature and many studies have shown that the endothelial cells and neovasculature are sensitive to these agents at concentrations lower than that required for cancer cells[18, 22, 33]. Clearly the PTX-M and RAP-M follow the same pattern at 20 mg/kg to produce antiangiogenic effects without apoptosis induction in the tumor tissue. Thus, based on our data we can use these individual micelles in a frequent dosing schedule and at a lower dose to target the tumor microenvironment instead of the cancer cells. We anticipate at higher doses and/or more frequent dosing both PTX-M and RAP-M will induce apoptosis as both compounds can produce such effects at specific doses in *in vitro* and *in vivo* models [79, 80]. MIX-M, however, showed duel antiangiogenic and apoptosis inducing effects leading to greater reduction in the tumor volume in comparison to saline, PEG-LEV, and individual micelles.

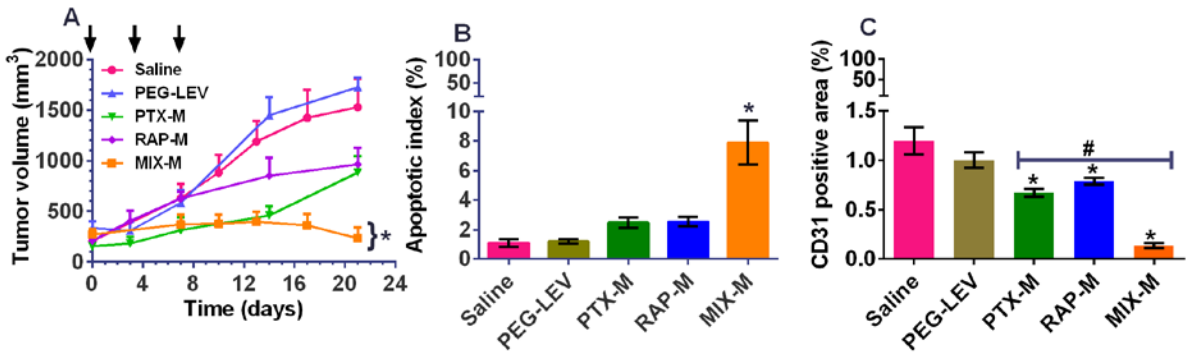

Fig. 8. Xenograft regression in mice over time after i.v. injection of saline (control), PEG-LEV, PTX-M, RAP-M, MIX-M at PTX and/or RAP at 20 mg/kg each on days 0, 4, and 8 as indicated by arrows (n = 5/treatment, Mean ± SD). Tumor volume (A), quantification of apoptotic cells in tumor tissue by counterstaining with anti-Caspase-3 antibody (B), quantification of microvessel in tumor tissue by counterstaining with anti-CD31 antibody (D31 positive) (C). * Represents significant difference from control (saline), # represents significant difference from MIX-M (Mean ± SD, n=5). Significant differences between treatment group means is evaluated using one way ANOVA with Dunnett's Multiple Comparison Test (compare all columns vs. control) or Bonferroni Multiple Comparison Test (compare all pairs of columns) using a significant level (α) of 0.05. Analysis is performed with GraphPad Prism version 5.04 for Windows, GraphPad Software, San Diego California USA

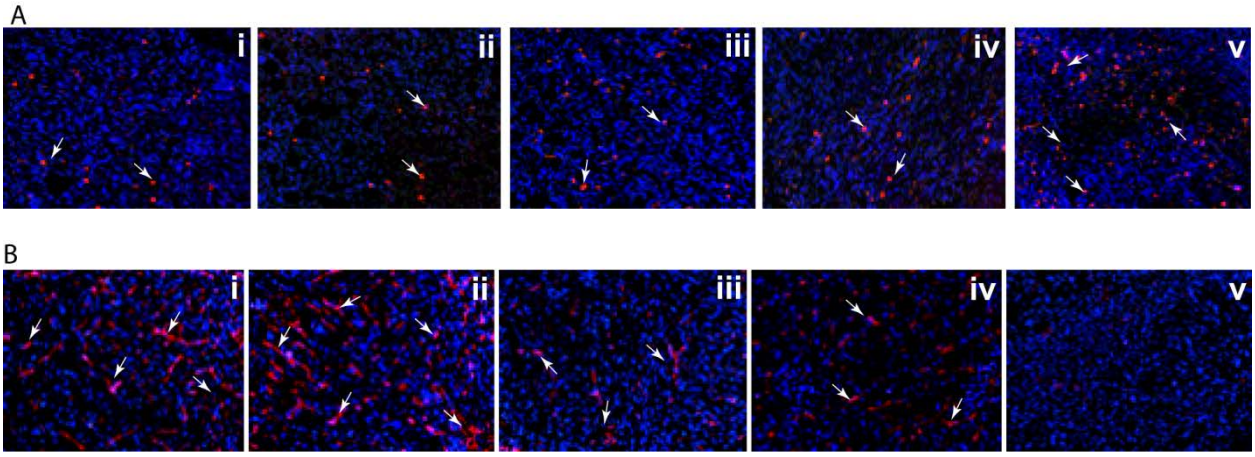

Fig. 9. ES2 ovarian cancer xenograft mice treated with saline (i), PEG-LEV (ii), PTX-M (iii), RAP-M (iv), and MIX-M (v). IHC staining for tumor-associated apoptotic cells (A) and Angiogenesis (B). Apoptotic cells are identified by counterstaining with anti-Caspase-3 antibody (red). Endothelial cells (angiogenesis) are identified by counterstaining with anti-CD31 antibody (red). Cells Nuclei are identified with DAPI staining (Blue).

Conclusions

Current chemotherapeutic strategies of dosing at MTD to treat solid tumors like ovarian cancer every 3 weeks [3, 4] allow the patient to recover from chemotherapy-induced adverse effects. However, this drug-free interval can promote tumor to reinitiate growth[5] through the mobilization of circulating endothelial progenitor cells and results in tumor neovascularization[3]. The MTD

chemotherapy in general is effective in cancers without a complex network of activating mutations such as gestational choriocarcinomas, testicular cancer, Hodgkin's disease, and B-cell non-Hodgkin's lymphoma[81]. Complex cancers such as ovarian, sarcoma, breast, prostate, and lung demonstrate poorer prognosis with conventional MTD treatment regimens[81]. New advances in tumor biology suggest targeting the tumor microenvironment and not just the cancer cells through anti-angiogenic agents and reactivating host immune responses may provide better outcomes in complex cancers[20]. Targeting angiogenesis is one of the corner stones of MR. Recent studies have shown that MR induces other mechanisms of actions including antitumor immune response and direct anticancer effects. Therefore, MR is now considered to be a form of multiple-targeted chemotherapy that has a profound effect on the tumor microenvironment. Conjugated micelles offer the ability to elicit multiple mechanisms of action for a drug which may be suppressed in conventional dosage forms. In our study, we have demonstrated, *in vitro* and *in vivo,* the safety and efficacy of the conjugated PTX, RAP, or PTX and RAP 1:1 mixed micelles in treating ovarian cancer through both cytotoxic effects in cancer cells and simultaneous inhibition of angiogenesis. Thus, offering a drug delivery system that can be tailored to different treatment paradigms like MTD dosing or MR. In addition, the MIX-M, through its synergistic activity, may also prove to be more effective in overcoming resistance issues commonly seen with other chemotherapeutic agents. Thus, the MIX-M micellar system can provide a platform that will allow clinicians to tailor therapy to tumor cells or the tumor microenvironment for the treatment of complex cancers like ovarian cancer.

Acknowledgement

This study was supported by the grant from AACP New Pharmacy Faculty Research Award Program, Medical Research Foundation of Oregon New Investigator Grant and Oregon State University-Startup fund. Electron microscopy was performed at the Multiscale Microscopy Core (MMC) with technical support from the Oregon Health & Science University (OHSU)-FEI Living Lab and the OHSU Center for Spatial Systems Biomedicine (OCSSB)

References

1. Jemal, A.; Murray, T.; Ward, E.; Samuels, A.; Tiwari, R. C.; Ghafoor, A.; Feuer, E. J.; Thun, M. J., Cancer statistics, 2005. *Ca-A Cancer Journal for Clinicians* **2005,** 55, (1), 10-30.

2. Cohn, D. E.; Valmadre, S.; Resnick, K. E.; Eaton, L. A.; Copeland, L. J.; Fowler, J. M., Bevacizumab and weekly taxane chemotherapy demonstrates activity in refractory ovarian cancer. *Gynecologic oncology* **2006,** 102, (2), 134-9.

3. Bertolini, F.; Paul, S.; Mancuso, P.; Monestiroli, S.; Gobbi, A.; Shaked, Y.; Kerbel, R. S., Maximum tolerable dose and low-dose metronomic chemotherapy have opposite effects on the mobilization and viability of circulating endothelial progenitor cells. *Cancer Res.* **2003,** 63, (15), 4342-6.

4. Shaked, Y.; Ciarrocchi, A.; Franco, M.; Lee, C. R.; Man, S.; Cheung, A. M.; Hicklin, D. J.; Chaplin, D.; Foster, F. S.; Benezra, R.; Kerbel, R. S., Therapy-induced acute recruitment of circulating endothelial progenitor cells to tumors. *Science (Washington, DC, U. S.)* **2006,** 313, (5794), 1785-7.

5. Kim, J. J.; Tannock, I. F., Repopulation of cancer cells during therapy: an important cause of treatment failure. *Nat. Rev. Cancer* **2005,** 5, (7), 516-25.

6. Kim, A.; Ueda, Y.; Naka, T.; Enomoto, T., Therapeutic strategies in epithelial ovarian cancer. *J Exp Clin Canc Res* **2012,** 31, 14-24.

7. Piccart, M. J.; Nogaret, J. M., Optimal therapeutic strategies in ovarian epithelial cancer in 1997. *Rev Med Brux* **1997,** 18, (4), 198-203.

8. Sounni, N. E.; Noel, A., Targeting the tumor microenvironment for cancer therapy. *Clin. Chem. (Washington, DC, U. S.)* **2013,** 59, (1), 85-93.

9. Tsai, M. J.; Chang, W. A.; Huang, M. S.; Kuo, P. L., Tumor microenvironment: a new treatment target for cancer. *ISRN biochemistry* **2014,** 2014, 1-9.

10. Bergers, G.; Hanahan, D., Modes of resistance to anti-angiogenic therapy. *Nat. Rev. Cancer* **2008,** 8, (8), 592-603.

11. Bocci, G.; Loupakis, F., The possible role of chemotherapy in antiangiogenic drug resistance. *Medical hypotheses* **2012,** 78, (5), 646-8.

12. Kerbel, R. S.; Yu, J.; Tran, J.; Man, S.; Viloria-Petit, A.; Klement, G.; Coomber, B. L.; Rak, J., Possible mechanisms of acquired resistance to anti-angiogenic drugs: Implications for the use of combination therapy approaches. *Cancer Metast Rev* **2001,** 20, (1-2), 79-86.

13. Loges, S.; Schmidt, T.; Carmeliet, P., Mechanisms of resistance to anti-angiogenic therapy and development of third-generation anti-angiogenic drug candidates. *Genes & cancer* **2010,** 1, (1), 12-25.

14. Karakus, G.; Akin Polat, Z.; Sahin Yaglioglu, A.; Karahan, M.; Yenidunya, A. F., Synthesis, characterization, and assessment of cytotoxic, antiproliferative, and antiangiogenic

effects of a novel procainamide hydrochloride-poly(maleic anhydride-co-styrene) conjugate. *J. Biomater. Sci., Polym. Ed.* **2013,** 24, (10), 1260-76.

15. Andre, N.; Carre, M.; Pasquier, E., Metronomics: towards personalized chemotherapy? *Nat. Rev. Clin. Oncol.* **2014,** 11, (7), 413-31.

16. Kerbel, R. S.; Kamen, B. A., The anti-angiogenic basis of metronomic chemotherapy. *Nat. Rev. Cancer* **2004,** 4, (6), 423-36.

17. Hanahan, D.; Bergers, G.; Bergsland, E., Less is more, regularly: metronomic dosing of cytotoxic drugs can target tumor angiogenesis in mice. *J. Clin. Invest.* **2000,** 105, (8), 1045-7.

18. Bocci, G.; Nicolaou, K. C.; Kerbel, R. S., Protracted low-dose effects on human endothelial cell proliferation and survival in vitro reveal a selective antiangiogenic window for various chemotherapeutic drugs. *Cancer Res.* **2002,** 62, (23), 6938-43.

19. Shaked, Y.; Emmenegger, U.; Man, S.; Cervi, D.; Bertolini, F.; Ben-David, Y.; Kerbel, R. S., Optimal biologic dose of metronomic chemotherapy regimens is associated with maximum antiangiogenic activity. *Blood* **2005,** 106, (9), 3058-61.

20. Pasquier, E.; Kavallaris, M.; Andre, N., Metronomic chemotherapy: new rationale for new directions. *Nat. Rev. Clin. Oncol.* **2010,** 7, (8), 455-65.

21. Ghiringhelli, F.; Menard, C.; Puig, P. E.; Ladoire, S.; Roux, S.; Martin, F.; Solary, E.; Le Cesne, A.; Zitvogel, L.; Chauffert, B., Metronomic cyclophosphamide regimen selectively depletes CD4+CD25+ regulatory T cells and restores T and NK effector functions in end stage cancer patients. *Cancer Immunol. Immunother.* **2007,** 56, (5), 641-8.

22. Guba, M.; von Breitenbuch, P.; Steinbauer, M.; Koehl, G.; Flegel, S.; Hornung, M.; Bruns, C. J.; Zuelke, C.; Farkas, S.; Anthuber, M.; Jauch, K. W.; Geissler, E. K., Rapamycin inhibits primary and metastatic tumor growth by antiangiogenesis: involvement of vascular endothelial growth factor. *Nat. Med. (N. Y., NY, U. S.)* **2002,** 8, (2), 128-35.

23. Ng, S. S.; Figg, W. D.; Sparreboom, A., Taxane-mediated antiangiogenesis *in vitro*: influence of formulation vehicles and binding proteins. *Cancer Res.* **2004,** 64, (3), 821-4.

24. Francia, G.; Man, S.; Lawler, J.; Kerbel, R. S., Thrombospondin 1, a mediator of the antiangiogenic effects of low-dose metronomic chemotherapy. *Proc. Natl. Acad. Sci. U. S. A.* **2003,** 100, 12917-22.

25. Miller, K. D.; Sweeney, C. J.; Sledge, G. W., Redefining the target: Chemotherapeutics as antiangiogenics. *J Clin Oncol* **2001,** 19, (4), 1195-1206.

26. Belotti, D.; Vergani, V.; Drudis, T.; Borsotti, P.; Pitelli, M. R.; Viale, G.; Giavazzi, R.; Taraboletti, G., The microtubule-affecting drug paclitaxel has antiangiogenic activity. *Clin. Cancer Res.* **1996,** 2, (11), 1843-1849.

27. Belotti, D.; Rieppi, M.; Nicoletti, M. I.; Casazza, A. M.; Fojo, T.; Taraboletti, G.; Giavazzi, R., Paclitaxel (Taxol(R)) inhibits motility of paclitaxel-resistant human ovarian carcinoma cells. *Clin. Cancer Res.* **1996,** 2, (10), 1725-30.

28. Belotti, D.; Vergani, V.; Drudis, T.; Borsotti, P.; Pitelli, M. R.; Viale, G.; Giavazzi, R.; Taraboletti, G., The microtubule-affecting drug paclitaxel has antiangiogenic activity. *Clin Cancer Res* **1996,** 2, (11), 1843-9.

29. Gao, H.; Zhang, J.; Liu, T.; Shi, W., Rapamycin prevents endothelial cell migration by inhibiting the endothelial-to-mesenchymal transition and matrix metalloproteinase-2 and -9: an in vitro study. *Mol. Vision* **2011,** 17, 3406-14.

30. Hay, N., The Akt-mTOR tango and its relevance to cancer. *Cancer cell* **2005,** 8, (3), 179-83.

31. Yap, T. A.; Garrett, M. D.; Walton, M. I.; Raynaud, F.; de Bono, J. S.; Workman, P., Targeting the PI3K-AKT-mTOR pathway: progress, pitfalls, and promises. *Curr. Opin. Pharmacol.* **2008,** 8, (4), 393-412.

32. Faivre, S.; Kroemer, G.; Raymond, E., Current development of mTOR inhibitors as anticancer agents. *Nat. Rev. Drug Discovery* **2006,** 5, (8), 671-88.

33. Mishra, G. P.; Nguyen, D.; Alani, A. W., Inhibitory effect of paclitaxel and rapamycin individual and dual drug-loaded polymeric micelles in the angiogenic cascade. *Mol. Pharmaceutics* **2013,** 10, (5), 2071-8.

34. Ellard, S. L.; Clemons, M.; Gelmon, K. A.; Norris, B.; Kennecke, H.; Chia, S.; Pritchard, K.; Eisen, A.; Vandenberg, T.; Taylor, M.; Sauerbrei, E.; Mishaeli, M.; Huntsman, D.; Walsh, W.; Olivo, M.; McIntosh, L.; Seymour, L., Randomized phase II study comparing two schedules of everolimus in patients with recurrent/metastatic breast cancer: NCIC Clinical Trials Group IND.163. *J Clin Oncol* **2009,** 27, (27), 4536-41.

35. Mita, M. M.; Mita, A. C.; Chu, Q. S.; Rowinsky, E. K.; Fetterly, G. J.; Goldston, M.; Patnaik, A.; Mathews, L.; Ricart, A. D.; Mays, T.; Knowles, H.; Rivera, V. M.; Kreisberg, J.; Bedrosian, C. L.; Tolcher, A. W., Phase I trial of the novel mammalian target of rapamycin inhibitor deforolimus (AP23573; MK-8669) administered intravenously daily for 5 days every 2 weeks to patients with advanced malignancies. *J Clin Oncol* **2008,** 26, (3), 361-7.

36. O'Donnell, A.; Faivre, S.; Burris, H. A., 3rd; Rea, D.; Papadimitrakopoulou, V.; Shand, N.; Lane, H. A.; Hazell, K.; Zoellner, U.; Kovarik, J. M.; Brock, C.; Jones, S.; Raymond, E.; Judson, I., Phase I pharmacokinetic and pharmacodynamic study of the oral mammalian target of rapamycin inhibitor everolimus in patients with advanced solid tumors. *J Clin Oncol* **2008,** 26, (10), 1588-95.

37. Biswas, S.; Kumari, P.; Lakhani, P. M.; Ghosh, B., Recent advances in polymeric micelles for anti-cancer drug delivery. *Eur. J. Pharm. Sci.* **2015**.

38. Gong, J.; Chen, M.; Zheng, Y.; Wang, S.; Wang, Y., Polymeric micelles drug delivery system in oncology. *J. Controlled Release* **2012,** 159, (3), 312-23.

39. Yokoyama, M.; Kwon, G. S.; Okano, T.; Sakurai, Y.; Seto, T.; Kataoka, K., Preparation of micelle-forming polymer-drug conjugates. *Bioconjugate Chem.* **1992,** 3, (4), 295-301.

40. Yokoyama, M.; Okano, T.; Sakurai, Y.; Kataoka, K., Improved synthesis of adriamycin-conjugated poly (ethylene oxide)-poly (aspartic acid) block copolymer and formation of unimodal

micellar structure with controlled amount of physically entrapped adriamycin. *J. Controlled Release* **1994,** 32, (3), 269-277.

41. Alani, A. W. G.; Bae, Y.; Kwon, G. S., Synthesis and characterization of a micellar drug carrier for the metronomic delivery of paclitaxel. *J. Controlled Release* **2008,** 132, e19-e20.

42. Alani, A. W.; Bae, Y.; Rao, D. A.; Kwon, G. S., Polymeric micelles for the pH-dependent controlled, continuous low dose release of paclitaxel. *Biomaterials* **2010,** 31, 1765-72.

43. Bae, Y.; Alani, A. W.; Rockich, N. C.; Lai, T. S.; Kwon, G. S., Mixed pH-sensitive polymeric micelles for combination drug delivery. *Pharm. Res.* **2010,** 27, (11), 2421-32.

44. Shin, H. C.; Alani, A. W.; Rao, D. A.; Rockich, N. C.; Kwon, G. S., Multi-drug loaded polymeric micelles for simultaneous delivery of poorly soluble anticancer drugs. *J. Controlled Release* **2009,** 140, (3), 294-300.

45. Shin, H. C.; Alani, A. W.; Cho, H.; Bae, Y.; Kolesar, J. M.; Kwon, G. S., A 3-in-1 polymeric micelle nanocontainer for poorly water-soluble drugs. *Mol. Pharmaceutics* **2011,** 8, (4), 1257-65.

46. Shaw, T. J.; Senterman, M. K.; Dawson, K.; Crane, C. A.; Vanderhyden, B. C., Characterization of intraperitoneal, orthotopic, and metastatic xenograft models of human ovarian cancer. *Mol. Ther.* **2004,** 10, (6), 1032-42.

47. Pectasides, D.; Pectasides, E.; Psyrri, A.; Economopoulos, T., Treatment issues in clear cell carcinoma of the ovary: a different entity? *Oncologist* **2006,** 11, (10), 1089-94.

48. Jaffe, E. A.; Nachman, R. L.; Becker, C. G.; Minick, C. R., Culture of human endothelial cells derived from umbilical veins. Identification by morphologic and immunologic criteria. *J. Clin. Invest.* **1973,** 52, (11), 2745-56.

49. Daly, W. H.; Poche, D., The Preparation of N-Carboxyanhydrides of Alpha-Amino-Acids Using Bis(Trichloromethyl)Carbonate. *Tetrahedron Lett* **1988,** 29, (46), 5859-5862.

50. Yokoyama, M.; Miyauchi, M.; Yamada, N.; Okano, T.; Sakurai, Y.; Kataoka, K.; Inoue, S., Polymer Micelles as Novel Drug Carrier - Adriamycin-Conjugated Poly(Ethylene Glycol) Poly(Aspartic Acid) Block Copolymer. *J. Controlled Release* **1990,** 11, (1-3), 269-278.

51. Yokoyama, M.; Miyauchi, M.; Yamada, N.; Okano, T.; Sakurai, Y.; Kataoka, K.; Inoue, S., Characterization and anticancer activity of the micelle-forming polymeric anticancer drug adriamycin-conjugated poly(ethylene glycol)-poly(aspartic acid) block copolymer. *Cancer Res.* **1990,** 50, (6), 1693-700.

52. Bae, Y.; Fukushima, S.; Harada, A.; Kataoka, K., Design of environment-sensitive supramolecular assemblies for intracellular drug delivery: polymeric micelles that are responsive to intracellular pH change. *Angew. Chem. Int. Ed.* **2003,** 42, (38), 4640-3.

53. Bae, Y.; Jang, W. D.; Nishiyama, N.; Fukushima, S.; Kataoka, K., Multifunctional polymeric micelles with folate-mediated cancer cell targeting and pH-triggered drug releasing properties for active intracellular drug delivery. *Mol. BioSyst.* **2005,** 1, (3), 242-50.

54. Bae, Y.; Nishiyama, N.; Kataoka, K., *In vivo* antitumor activity of the folate-conjugated pH-sensitive polymeric micelle selectively releasing adriamycin in the intracellular acidic compartments. *Bioconjugate Chem.* **2007,** 18, (4), 1131-9.

55. Chou, T.-C.; Martin, N. *CompuSyn*, 1.0; ComboSyn, Inc., Paramus, NJ 2007.

56. Chou, T. C.; Talalay, P., Quantitative analysis of dose-effect relationships: the combined effects of multiple drugs or enzyme inhibitors. *Adv. Enzyme Regul.* **1984,** 22, (0), 27-55.

57. Wang, Z.; Kirkwood, J. S.; Taylor, A. W.; Stevens, J. F.; Leid, M.; Ganguli-Indra, G.; Indra, A. K., Transcription factor Ctip2 controls epidermal lipid metabolism and regulates expression of genes involved in sphingolipid biosynthesis during skin development. *J. Invest. Dermatol.* **2013,** 133, (3), 668-76.

58. Cammas-Marion, S.; Okano, T.; Kataoka, K., Functional and site-specific macromolecular micelles as high potential drug carriers. *Colloids Surf., B* **1999,** 16, (1–4), 207-215.

59. Benjamin, D.; Colombi, M.; Moroni, C.; Hall, M. N., Rapamycin passes the torch: a new generation of mTOR inhibitors. *Nat. Rev. Drug Discovery* **2011,** 10, (11), 868-80.

60. Lu, Y.; An, L.; Wang, Z.-G., Intrinsic Viscosity of Polymers: General Theory Based on a Partially Permeable Sphere Model. *Macromolecules (Washington, DC, U. S.)* **2013,** 46, (14), 5731-5740.

61. Armstrong, J. K.; Wenby, R. B.; Meiselman, H. J.; Fisher, T. C., The hydrodynamic radii of macromolecules and their effect on red blood cell aggregation. *Biophys J* **2004,** 87, (6), 4259-70.

62. Lapasin, R.; Pricl, S., Rheology of polysaccharide systems. In *Rheology of industrial polysaccharides: theory and applications*, 1995; pp 273-274.

63. Owen, S. C.; Chan, D. P. Y.; Shoichet, M. S., Polymeric micelle stability. *Nano Today* **2012,** 7, (1), 53-65.

64. Bae, Y.; Diezi, T. A.; Zhao, A.; Kwon, G. S., Mixed polymeric micelles for combination cancer chemotherapy through the concurrent delivery of multiple chemotherapeutic agents. *J. Controlled Release* **2007,** 122, (3), 324-30.

65. Rowinsky, E. K., Clinical pharmacology of Taxol. *J. Natl. Cancer Inst. Monogr.* **1993**, (15), 25-37.

66. Rowinsky, E. K.; Donehower, R. C., Paclitaxel (taxol). *N. Engl. J. Med.* **1995,** 332, (15), 1004-14.

67. Liu, Q. J.; Xu, X. H.; Shang, D. H.; Tian, Y.; Lu, W. C.; Zhang, Y. H., Rapamycin enhances the susceptibility of both androgen-dependent and -independent prostate carcinoma cells to docetaxel. *Chin. Med. J. (Beijing, China, Engl. Ed.)* **2010,** 123, (3), 356-60.

68. Ma, X. Y.; Wang, S. X.; Liu, Y.; Liu, R. H.; Lu, Y. P.; Ma, D., [Induction effect of rapamycin combined paclitaxel on apoptosis of ovarian cancer cell lines A2780 and SKOV3 and the molecular mechanism]. *Aizheng* **2007,** 26, (4), 367-70.

69. Shafer, A.; Zhou, C.; Gehrig, P. A.; Boggess, J. F.; Bae-Jump, V. L., Rapamycin potentiates the effects of paclitaxel in endometrial cancer cells through inhibition of cell proliferation and induction of apoptosis. *Int. J. Cancer* **2010,** 126, (5), 1144-54.

70. Parry, T. J.; Brosius, R.; Thyagarajan, R.; Carter, D.; Argentieri, D.; Falotico, R.; Siekierka, J., Drug-eluting stents: sirolimus and paclitaxel differentially affect cultured cells and injured arteries. *Eur. J. Pharmacol.* **2005,** 524, (1-3), 19-29.

71. Hotchkiss, K. A.; Ashton, A. W.; Mahmood, R.; Russell, R. G.; Sparano, J. A.; Schwartz, E. L., Inhibition of endothelial cell function in vitro and angiogenesis in vivo by docetaxel (Taxotere): association with impaired repositioning of the microtubule organizing center. *Mol. Cancer Ther.* **2002,** 1, (13), 1191-200.

72. Papetti, M.; Herman, I. M., Mechanisms of normal and tumor-derived angiogenesis. *Am. J. Physiol.: Cell Physiol.* **2002,** 282, (5), C947-70.

73. Trail, P. A.; Willner, D.; Bianchi, A. B.; Henderson, A. J.; TrailSmith, M. D.; Girit, E.; Lasch, S.; Hellstrom, I.; Hellstrom, K. E., Enhanced antitumor activity of paclitaxel in combination with the anticarcinoma immunoconjugate BR96-doxorubicin. *Clin. Cancer Res.* **1999,** 5, (11), 3632-8.

74. Desai, N.; Trieu, V.; Soon-Shiong, P.; Hawkins, M., Abraxane (ABI-007) vs taxotere: a preclinical comparison of toxicity and efficacy. *Cancer Res.* **2005,** 65, (9 Supplement), 336-337.

75. Kim, S. C.; Kim, D. W.; Shim, Y. H.; Bang, J. S.; Oh, H. S.; Wan Kim, S.; Seo, M. H., In vivo evaluation of polymeric micellar paclitaxel formulation: toxicity and efficacy. *J. Controlled Release* **2001,** 72, (1-3), 191-202.

76. ClinicalTrials.gov Bioequivalence Study of IG-001 Versus Nab-paclitaxel in Metastatic or Locally Recurrent Breast Cancer (TRIBECA).

77. Houghton, P. J.; Morton, C. L.; Gorlick, R.; Lock, R. B.; Carol, H.; Reynolds, C. P.; Kang, M. H.; Maris, J. M.; Keir, S. T.; Kolb, E. A.; Wu, J.; Wozniak, A. W.; Billups, C. A.; Rubinstein, L.; Smith, M. A., Stage 2 combination testing of rapamycin with cytotoxic agents by the Pediatric Preclinical Testing Program. *Mol. Cancer Ther.* **2010,** 9, (1), 101-12.

78. Fernandes-Alnemri, T.; Litwack, G.; Alnemri, E. S., CPP32, a novel human apoptotic protein with homology to Caenorhabditis elegans cell death protein Ced-3 and mammalian interleukin-1 beta-converting enzyme. *J. Biol. Chem.* **1994,** 269, (49), 30761-4.

79. Vassileva, V.; Allen, C. J.; Piquette-Miller, M., Effects of sustained and intermittent paclitaxel therapy on tumor repopulation in ovarian cancer. *Mol. Cancer Ther.* **2008,** 7, (3), 630-7.

80. Frost, P.; Berlanger, E.; Mysore, V.; Hoang, B.; Shi, Y.; Gera, J.; Lichtenstein, A., Mammalian target of rapamycin inhibitors induce tumor cell apoptosis in vivo primarily by inhibiting VEGF expression and angiogenesis. *J. Oncol.* **2013,** 2013, 1-12.

81. Kareva, I.; Waxman, D. J.; Lakka Klement, G., Metronomic chemotherapy: an attractive alternative to maximum tolerated dose therapy that can activate anti-tumor immunity and minimize therapeutic resistance. *Cancer Lett. (N. Y., NY, U. S.)* **2015,** 358, (2), 100-6.